IEEE Access
Multidisciplinary | Rapid Review | Open Access Journal

Received November 27, 2019, accepted December 17, 2019, date of publication December 25, 2019,
date of current version January 6, 2020.

Digital Object Identifier 10.1109/ACCESS.2019.2962187

Modeling and Analysis of the Electro-Optic Modulator With Alignment Errors

PENG ZHANG, XIAOPING DU, AND YISHUO SONG
Space Engineering University, Beijing 101416, China

Corresponding author: Peng Zhang (zhangjypeng@163.com)

This work was supported by the National Natural Science Foundation of China under Grant No 61805284.

ABSTRACT Electro-optic modulators have enabled a wide range of emerging applications that place greater demands on the alignment of the modulators. In this paper, for the first time to the best of our knowledge, we construct a theoretical model to describe the electro-optic modulator with alignment errors, which helps us to quantitatively analyze the distribution characteristics of the exiting intensity of the electro-optic modulator under different alignment errors and different applied voltages. The alignment errors in the theoretical model are divided into three kinds, namely, the horizontal error, the vertical error, and the rotation error. The theoretical results show that the model and the distribution characteristics of the exiting intensity are useful to align the electro-optic modulator precisely in practical applications. Furthermore, an experimental setup is proposed to align the electro-optic modulator based on a lithium niobite crystal and to verify the correctness of the model presented in this paper. An excellent agreement is found between the theoretical results and the experimental results.

INDEX TERMS Electro-optic modulator, alignment error, polarization ray tracing.

I. INTRODUCTION

Electro-optic modulators are the engines of the classical optical communication systems, which convert the electrical signals to optical signals by varying the phase or intensity of the normal incident light beam [1]. In recent years, electro-optic modulators have enabled a wide range of emerging applications, including quantum information networks [2], wide-field fluorescence lifetime microscopy [3], free-space optical communications [4], high-resolution LIDAR systems [5], [6], and so on. In these emerging applications, electro-optic modulators should be designed to modulate not only the normal incident light beams but also the tilt incident light beams. Due to the nature birefringent of the electro-optic crystals are very sensitive to the incident directions of the light beams, high precision manufacturing and alignment of electro-optic modulators are crucial to these emerging applications [7]–[9]. Therefore, it is of great importance to establish the theoretical model to provide guidance in fabricating and mounting the electro-optic modulators. The current models for electro-optic modulators are mainly based on Jones calculus and Mueller calculus [8], [10]–[12], which have two unsolved issues: 1) the Jones calculus and the Mueller calculus are defined for the light beam when the polarization paraxial approximation holds, which means they are only suitable for describing the normal incident light beam; 2) Only a small misalignment in the rotation angles of the electro-optic crystal was described, namely, the alignment errors of the electro-optic crystal have not been fully considered.

In our previous work, we derived the analytical formulas of the parameters to describe the light beam propagation characteristics in electro-optic crystals with an arbitrary incident direction [13]. On this basis, this paper uses the three-dimensional polarization ray tracing calculus to build the theoretical model of the electro-optic modulator with three kinds of alignment errors.

In Section II of this paper, we present our theoretical model. For clarity, we divide Section II into three subsections. In the first subsection, the horizontal error, the vertical error, and the rotation error are described. In the second subsection, we describe the analytical formulas for a ray through the electro-optic crystal with an arbitrary incident direction. In the third subsection, we applied the three-dimensional polarization ray tracing calculus to describe the exiting intensity of the modulator. Then, an electro-optic modulator based

The associate editor coordinating the review of this manuscript and approving it for publication was Wen-Sheng Zhao.

This work is licensed under a Creative Commons Attribution 4.0 License. For more information, see http://creativecommons.org/licenses/by/4.0/

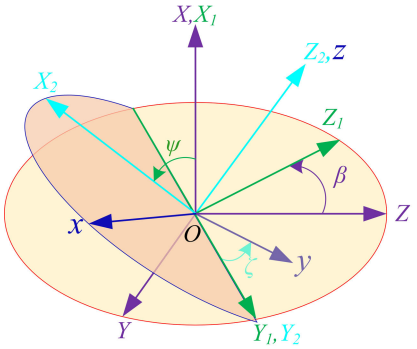

FIGURE 1. The relationship between the three-dimensional global coordinate system (*X, Y, Z*) and the coordinate system for the field-free principal dielectric axes of an electro-optic crystal (*x, y, z*): β is the horizontal error angle; ψ is the vertical error angle; ζ is the rotation error angle.

on a lithium niobite crystal is considered as an example and the results are discussed in Section III. Finally, the conclusions are summarized in Section IV.

II. THEORETICAL MODEL

A. ALIGNMENT ERRORS OF THE ELECTRO-OPTIC CRYSTAL

Under the ideal alignment condition, the optical axis of the electro-optic modulator should be parallel to the normal direction of the electro-optic crystal interface and the principal dielectric axes of the electro-optic crystal should be oriented towards specific directions corresponding to the transmission axis of the polarizer in the electro-optic modulator. In order to describe the alignment errors, two Cartesian coordinate systems are defined in this paper.

As shown in Figure 1, a Cartesian coordinate system X, Y, Z is defined as the global coordinate system of the electro-optic modulator in three-dimensional space. The optical axis of the electro-optic modulator is coincident with the Z-axis. Meanwhile, the other Cartesian coordinate system x, y, z is defined as the principal dielectric axes of the electro-optic crystal. The normal direction of the crystal interface is parallel to the z-axis. When the electro-optic crystal is imperfectly installed, the X, Y, Z coordinate system is not coincident with the x, y, z coordinate system. The relationship between these two coordinate systems can be described by rotational coordinate transformations. First, we rotate from the global three-dimensional coordinate system X, Y, Z into an X_1, Y_1, Z_1 coordinate system through a rotation β about the X-axis. Let $\hat{\mathbf{X}}$, $\hat{\mathbf{Y}}$, $\hat{\mathbf{Z}}$ and $\hat{\mathbf{X}}_\mathbf{1}$, $\hat{\mathbf{Y}}_\mathbf{1}$, $\hat{\mathbf{Z}}_\mathbf{1}$ be the unit vectors along the X-, Y-, Z-axis, and the X_1-, Y_1-, Z_1-axis. The relationship between the unit vectors $\hat{\mathbf{X}}$, $\hat{\mathbf{Y}}$, $\hat{\mathbf{Z}}$ and the unit vectors $\hat{\mathbf{X}}_\mathbf{1}$, $\hat{\mathbf{Y}}_\mathbf{1}$, $\hat{\mathbf{Z}}_\mathbf{1}$ can be defined as

$$\begin{aligned}\begin{pmatrix}\hat{\mathbf{X}}_\mathbf{1} & \hat{\mathbf{Y}}_\mathbf{1} & \hat{\mathbf{Z}}_\mathbf{1}\end{pmatrix} &= \begin{pmatrix}\hat{\mathbf{X}} & \hat{\mathbf{Y}} & \hat{\mathbf{Z}}\end{pmatrix}\begin{bmatrix}1 & 0 & 0\\ 0 & \cos\beta & -\sin\beta\\ 0 & \sin\beta & \cos\beta\end{bmatrix}\\ &= \begin{pmatrix}\hat{\mathbf{X}} & \hat{\mathbf{Y}} & \hat{\mathbf{Z}}\end{pmatrix}\cdot\mathbf{T}_1. \end{aligned} \tag{1}$$

The resulting Y_1-axis and Z_1-axis remain in the OYZ plane. Then, we rotate about the Y_1-axis into the X_2, Y_2, Z_2 coordinate system through an angle ψ. The Y_2-axis remains coincident with the Y_1-axis. The plane containing the Y_2-, Z_2- coordinate axis is now tipped through an angle ψ relative to the original OYZ plane. The relationship between the unit vectors $\hat{\mathbf{X}}_\mathbf{1}$, $\hat{\mathbf{Y}}_\mathbf{1}$, $\hat{\mathbf{Z}}_\mathbf{1}$ and the unit vectors $\left(\hat{\mathbf{X}}_\mathbf{2}, \hat{\mathbf{Y}}_\mathbf{2}, \hat{\mathbf{Z}}_\mathbf{2}\right)$ which are along the X_2-, Y_2-, Z_2-axis can be expressed as

$$\begin{aligned}\begin{pmatrix}\hat{\mathbf{X}}_\mathbf{2} & \hat{\mathbf{Y}}_\mathbf{2} & \hat{\mathbf{Z}}_\mathbf{2}\end{pmatrix} &= \begin{pmatrix}\hat{\mathbf{X}}_\mathbf{1} & \hat{\mathbf{Y}}_\mathbf{1} & \hat{\mathbf{Z}}_\mathbf{1}\end{pmatrix}\begin{bmatrix}\cos\psi & 0 & \sin\psi\\ 0 & 1 & 0\\ -\sin\psi & 0 & \cos\psi\end{bmatrix}\\ &= \begin{pmatrix}\hat{\mathbf{X}}_\mathbf{1} & \hat{\mathbf{Y}}_\mathbf{1} & \hat{\mathbf{Z}}_\mathbf{1}\end{pmatrix}\cdot\mathbf{T}_2. \end{aligned} \tag{2}$$

And finally, we rotate about the Z_2 axis through an angle ζ into the coordinate system for the field-free principal dielectric axes of an electro-optic crystal (x, y, z). The z-axis is coincident with the Z_2-axis. The relationship between the unit vectors $\hat{\mathbf{X}}_\mathbf{2}$, $\hat{\mathbf{Y}}_\mathbf{2}$, $\hat{\mathbf{Z}}_\mathbf{2}$ and the unit vectors $\hat{\mathbf{x}}$, $\hat{\mathbf{y}}$, $\hat{\mathbf{z}}$ which are along the x-, y-, and z-axis of the coordinate system can be described as

$$\begin{aligned}\begin{pmatrix}\hat{\mathbf{x}} & \hat{\mathbf{y}} & \hat{\mathbf{z}}\end{pmatrix} &= \begin{pmatrix}\hat{\mathbf{X}}_\mathbf{2} & \hat{\mathbf{Y}}_\mathbf{2} & \hat{\mathbf{Z}}_\mathbf{2}\end{pmatrix}\begin{bmatrix}\cos\zeta & -\sin\zeta & 0\\ \sin\zeta & \cos\zeta & 0\\ 0 & 0 & 1\end{bmatrix}\\ &= \begin{pmatrix}\hat{\mathbf{X}}_\mathbf{2} & \hat{\mathbf{Y}}_\mathbf{2} & \hat{\mathbf{Z}}_\mathbf{2}\end{pmatrix}\cdot\mathbf{T}_3. \end{aligned} \tag{3}$$

We consider the transformation matrix between the unit vectors $\hat{\mathbf{x}}$, $\hat{\mathbf{y}}$, $\hat{\mathbf{z}}$ and the unit vectors $\hat{\mathbf{X}}$, $\hat{\mathbf{Y}}$, $\hat{\mathbf{Z}}$ is $\mathbf{T_{GC}}$. Utilizing Eqs.(1)–(3), the relationship between $\hat{\mathbf{x}}$, $\hat{\mathbf{y}}$, $\hat{\mathbf{z}}$ and $\hat{\mathbf{X}}$, $\hat{\mathbf{Y}}$, $\hat{\mathbf{Z}}$ can be expressed as

$$\begin{pmatrix}\hat{\mathbf{x}} & \hat{\mathbf{y}} & \hat{\mathbf{z}}\end{pmatrix} = \begin{pmatrix}\hat{\mathbf{X}} & \hat{\mathbf{Y}} & \hat{\mathbf{Z}}\end{pmatrix}\cdot\mathbf{T}_1\cdot\mathbf{T}_2\cdot\mathbf{T}_3. \tag{4}$$

Consequently, the transformation matrix $\mathbf{T_{GC}}$ is given by

$$\mathbf{T_{GC}} = \mathbf{T}_1\cdot\mathbf{T}_2\cdot\mathbf{T}_3. \tag{5}$$

It is worth noting that $\mathbf{T_{GC}}$ consists of the parameters β, ψ, and ζ. Here, the angle β represents the horizontal error, the angle ψ represents the vertical error, and the angle ζ represents the rotation error.

Consider a ray at the center of the incident light beam refracts from an isotropic medium into an electro-optic crystal plane plate. As shown in FIGURE 2, the wave vector of the incident light is $\mathbf{k_{in}}$, α_G represents the angle between $\mathbf{k_{in}}$ and the Z-axis, where $0° \le \alpha_G \le 90°$. The angle between the $Y{=}0$ plane and the plane which contains the incident wave vector $\mathbf{k_{in}}$ and the Z-axis is represented by ϕ_G which ranges from 0° to 360°. For a ray propagate along an arbitrary direction, the unit wave vector of the incident ray can be expressed as

$$\hat{\mathbf{k}}_\mathbf{in} = \begin{pmatrix}\hat{\mathbf{X}} & \hat{\mathbf{Y}} & \hat{\mathbf{Z}}\end{pmatrix}\begin{bmatrix}\sin\alpha_G\cos\phi_G\\ \sin\alpha_G\sin\phi_G\\ \cos\alpha_G\end{bmatrix}, \tag{6}$$

Substituting Eq.(4) and Eq.(5) into Eq.(6), we can obtain the following equation:

$$\begin{aligned}\hat{\mathbf{k}}_{\mathbf{in}} &= \begin{pmatrix}\hat{\mathbf{x}} & \hat{\mathbf{y}} & \hat{\mathbf{z}}\end{pmatrix} \mathbf{T}_{\mathbf{GL}}^{-1} \begin{bmatrix}\sin\alpha_G\cos\phi_G \\ \sin\alpha_G\sin\phi_G \\ \cos\alpha_G\end{bmatrix} \\ &= \begin{pmatrix}\hat{\mathbf{x}} & \hat{\mathbf{y}} & \hat{\mathbf{z}}\end{pmatrix} \begin{bmatrix}k_{inX} \\ k_{inY} \\ k_{inZ}\end{bmatrix}. \end{aligned} \tag{7}$$

where k_{inX}, k_{inY} and k_{inZ} are three components of $\hat{\mathbf{k}}\mathbf{in}$ in the x, y, z coordinate system.

Besides, the unit wave vector of the incident ray can also be described by the incidence angle α and the azimuth angle ϕ in the x, y, z coordinate system:

$$\hat{\mathbf{k}}_{\mathbf{in}} = \begin{pmatrix}\hat{\mathbf{x}} & \hat{\mathbf{y}} & \hat{\mathbf{z}}\end{pmatrix} \begin{bmatrix}\sin\alpha\cos\phi \\ \sin\alpha\sin\phi \\ \cos\alpha\end{bmatrix}. \tag{8}$$

Comparing Eq. (8) with Eq. (7), we can get the following equations for the incidence angle and the azimuth angle:

$$\alpha = \arccos\left(k_{inZ}\right). \tag{9}$$

$$\sin\phi = \frac{k_{inY}}{\sqrt{1-k_{inZ}^2}}, \quad \cos\phi = \frac{k_{inX}}{\sqrt{1-k_{inZ}^2}}. \tag{10}$$

B. ANALYTICAL FORMULAS FOR A RAY THROUGH THE ELECTRO-OPTIC CRYSTAL WITH AN ARBITRARY INCIDENT DIRECTION

Refraction in uniaxial crystals generally gives rise to two refracted rays: an ordinary ray, which follows Snell's law, and an extraordinary ray, which does not follow Snell's law. Nevertheless, when the crystal is biaxial symmetry, the two refracted rays are both extraordinary rays. The complexity of describing the propagation direction of the extraordinary ray lies in the fact that first the refractive index of the extraordinary ray varies in space, and second, the wave vector of the extraordinary ray is in general not parallel to its Poynting vector.

Due to a field-free uniaxial crystal generally becomes biaxial symmetry and the principal dielectric axes of the crystal rotate under the influence of an applied electric field, the task to describe the refraction in an electro-optic crystal is more complicated. For ease of description, the two refracted rays in the electro-optic crystal are represented by ray A and ray B, respectively. As shown in FIGURE 2, the two refracted rays propagate along different directions in the electro-optic crystal. Although the extraordinary ray does not follow Snell's law, the refraction in electro-optic crystals can also be described by the electromagnetic wave theory. In our previous work, according to the refractive index ellipsoid theory and the electromagnetic wave theory, we derived a set of analytical formulas to calculate the refractive indices, the wave vectors, and Poynting vectors of the two refracted rays in electro-optic crystals with an arbitrary incident direction [13]. The refractive indices of the ray A and ray B can be

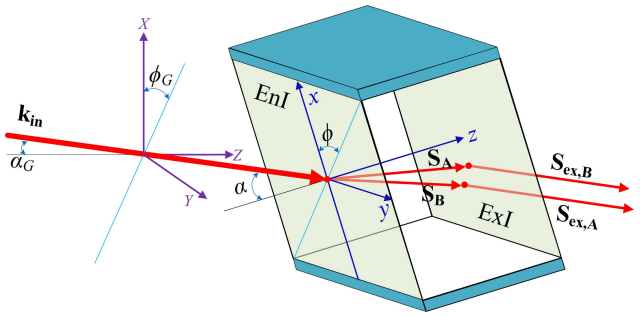

FIGURE 2. The propagation of a ray passing through the electro-optic crystal with an arbitrary direction. EnI: Entrance interface; ExI: Exit interface; $\mathbf{S_A}$, $\mathbf{S_B}$ are the Poynting vectors of the refracted ray A and the refracted ray B; $\mathbf{S_{ex,A}}$ and $\mathbf{S_{ex,B}}$ are the Poynting vectors of the exiting ray A and the exiting ray B.

calculated by the following equations:

$$n_A = \sqrt{\frac{B+\sqrt{B^2-4AC}}{2A}}, \tag{11}$$

$$n_B = \sqrt{\frac{B-\sqrt{B^2-4AC}}{2A}}. \tag{12}$$

with the parameters:

$$A = n_e^2, \tag{13}$$

$$\begin{aligned}B = {} & 2n_e^2\left(n_o^2+n_E^2\right) - n_i^2\sin^2\alpha\left(n_o^2-n_e^2+n_E^2\right) \\ & - 2n_o n_E n_i^2\sin^2\alpha \\ & \times\left[\left(1-2\sin^2\phi\right)\cos 2\theta + 2\sin\phi\cos\phi\sin 2\theta\right],\end{aligned} \tag{14}$$

$$\begin{aligned}C = {} & \left(n_o^2-n_E^2\right)^2 n_e^2 + n_i^2\sin^2\alpha \\ & \times\left[\left(n_o^2+n_E^2\right)n_e^2 - \left(n_o^2-n_E^2\right)^2\right] \\ & - 2n_o n_E n_e^2 n_i^2\sin^2\alpha \\ & \times\left[\left(1-2\sin^2\phi\right)\cos 2\theta + 2\sin\phi\cos\phi\sin 2\theta\right].\end{aligned} \tag{15}$$

where n_o and n_e are the ordinary refractive index and the extraordinary refractive index of the field free electro-optic crystal, respectively; n_i is the refractive index of the light in the isotropic medium; n_E is the change of refractive index induced by the applied electric field; θ is the rotation angle of the principal dielectric axes when the electric field is applied on the crystal.

Expressions which allow calculation of the wave vectors of the refracted rays in the electro-optic crystal are functions of the refractive indices, the incidence angle, and the azimuth angle. The unit wave vectors of the two refracted rays can be expressed as:

$$\hat{\mathbf{k}}_{\mathbf{A}} = \begin{pmatrix}\hat{\mathbf{x}} & \hat{\mathbf{y}} & \hat{\mathbf{z}}\end{pmatrix} \begin{bmatrix}n_i\sin\alpha\cos\phi/n_A \\ n_i\sin\alpha\sin\phi/n_A \\ \sqrt{1-n_i^2\sin^2\alpha/n_A^2}\end{bmatrix}. \tag{16}$$

$$\hat{\mathbf{k}}_{\mathbf{B}} = \begin{pmatrix} \hat{\mathbf{x}} & \hat{\mathbf{y}} & \hat{\mathbf{z}} \end{pmatrix} \begin{bmatrix} n_i \sin\alpha \cos\phi / n_B \\ n_i \sin\alpha \sin\phi / n_B \\ \sqrt{1 - n_i^2 \sin^2\alpha / n_B^2} \end{bmatrix}. \tag{17}$$

For a ray with the refractive index n in an electro-optic crystal, the Poynting vector of a refracted ray depends on the refractive index and the corresponding wave vector $\mathbf{k}$. The equation for the Poynting vector can be described by

$$\mathbf{S} = \begin{pmatrix} \hat{\mathbf{x}}_1 & \hat{\mathbf{x}}_2 & \hat{\mathbf{x}}_3 \end{pmatrix} \begin{bmatrix} \dfrac{(1+H)\, n_1^2 - n^2}{\sqrt{1+H\left(n_1^2 - n^2\right)}} \left(\mathbf{k} \cdot \hat{\mathbf{x}}_1\right) \\ \dfrac{(1+H)\, n_2^2 - n^2}{\sqrt{1+H\left(n_2^2 - n^2\right)}} \left(\mathbf{k} \cdot \hat{\mathbf{x}}_2\right) \\ \dfrac{(1+H)\, n_3^2 - n^2}{\sqrt{1+H\left(n_3^2 - n^2\right)}} \left(\mathbf{k} \cdot \hat{\mathbf{x}}_3\right) \end{bmatrix}, \tag{18}$$

where the auxiliary factor is

$$H = \left[\sum_1^3 n_j^4 \left(\mathbf{k} \cdot \hat{\mathbf{x}}_j\right)^2 / \left(n^2 - n_j^2\right)^2 \right]^{-1}. \tag{19}$$

where $\hat{\mathbf{x}}_1, \hat{\mathbf{x}}_2, \hat{\mathbf{x}}_3$ are the unit vectors along the electric field induced principal dielectric axes of the electro-optic crystal. The relationship between the unit vectors $\hat{\mathbf{x}}_1, \hat{\mathbf{x}}_2, \hat{\mathbf{x}}_3$ and $\hat{\mathbf{x}}, \hat{\mathbf{y}}, \hat{\mathbf{z}}$ can be expressed as

$$\left(\hat{\mathbf{x}}_1, \hat{\mathbf{x}}_2, \hat{\mathbf{x}}_3\right) = \left(\hat{\mathbf{x}}, \hat{\mathbf{y}}, \hat{\mathbf{z}}\right) \begin{bmatrix} \cos\theta & -\sin\theta & 0 \\ \sin\theta & \cos\theta & 0 \\ 0 & 0 & 1 \end{bmatrix}. \tag{20}$$

Therefore, substituting the expressions for the refractive indices and the wave vectors of the two refracted rays into Eq. (18) and Eq (19), we can obtain the Poynting vector of the ray A($\mathbf{S_A}$) and the Poynting vector of the ray B ($\mathbf{S_B}$). In an electro-optic crystal, the energy flux propagates along the Poynting vector, while the phase increase along the wave vector. Because of the wave vector is generally separated from its Poynting vector in the electro-optic crystal, the optical path lengths of the ray A and the ray B in the electro-optic crystal can be described as

$$OPL_A = n_A L \frac{\left(\hat{\mathbf{k}}_{\mathbf{A}} \cdot \mathbf{S_A}\right)}{\left(\mathbf{S_A} \cdot \hat{\mathbf{z}}\right)}. \tag{21}$$

$$OPL_B = n_B L \frac{\left(\hat{\mathbf{k}}_{\mathbf{B}} \cdot \mathbf{S_B}\right)}{\left(\mathbf{S_B} \cdot \hat{\mathbf{z}}\right)}. \tag{22}$$

C. THREE-DIMENSIONAL POLARIZATION RAY TRACING CALCULUS FOR THE ELECTRO-OPTIC MODULATOR

On the basis of Subsections (A) and (B), the evolution of the polarization state along a ray path through the electro-optic modulator should be further precisely quantified. Because of the incident direction is arbitrary, it is more convenient to quantify the evolution of the polarization state in three-dimensional space. The three-dimensional polarization ray tracing calculus is a generalization of the two-dimensional Jones calculus into the three-dimensional global coordinate system [14]. In the calculus, the polarization state is described by a 3×1 polarization vector and the changes in the polarization state are characterized by a series of 3×3 polarization ray tracing matrices. The polarization vector of the incident ray can be characterized by $\mathbf{E_0}$ [15]:

$$\mathbf{E_0} = E_0 \exp\left(i\phi_0\right) \hat{\mathbf{E}}_\mathbf{0}, \tag{23}$$

where $E_0 \exp(i\varphi_0)$ is the complex magnitude of incident polarization vector $\mathbf{E_0}$; $\hat{\mathbf{E}}_\mathbf{0}$ is the unit direction vector which satisfies the following equation:

$$\hat{\mathbf{E}}_\mathbf{0} \cdot \hat{\mathbf{E}}_\mathbf{0}^* = |E_x|^2 + \left|E_y\right|^2 + |E_z|^2 = 1. \tag{24}$$

Referring again to FIGURE 2, when the ray at the center of the incident light beam passes through the crystal, the evolution of polarization state consists of three parts, namely, the interaction between the ray and the entrance interface, the phase accumulation between the entrance interface and the exit interface, and the interaction between the ray and the exit interface. Due to the refraction in the electro-optic crystal gives rise to the ray A and the ray B, two polarization ray tracing matrices should be used to characterize the interaction between the incident ray and the entrance interface. The unit Poynting vector of the incident ray is $\hat{\mathbf{S}}\mathbf{in}$ which is equal to its unit wave vector $\hat{\mathbf{k}}\mathbf{in}$. In the isotropic medium, two orthogonal eigenmodes (s-polarization state and p-polarization state) can be expressed as

$$\hat{\mathbf{E}}_\mathbf{s} = \frac{\hat{\mathbf{S}}_\mathbf{in} \times \hat{\mathbf{z}}}{\left|\hat{\mathbf{S}}_\mathbf{in} \times \hat{\mathbf{z}}\right|}, \quad \hat{\mathbf{E}}_\mathbf{p} = \frac{\hat{\mathbf{S}}_\mathbf{in} \times \hat{\mathbf{E}}_\mathbf{s}}{\left|\hat{\mathbf{S}}_\mathbf{in} \times \hat{\mathbf{E}}_\mathbf{s}\right|}. \tag{25}$$

We consider the two refracted rays are polarized in $\hat{\mathbf{E}}_\mathbf{A}$ and $\hat{\mathbf{E}}_\mathbf{B}$, respectively. The unit Poynting vectors of the two refracted rays are represented by $\hat{\mathbf{S}}\mathbf{A}$ and $\hat{\mathbf{S}}\mathbf{B}$. According to Reference [16], the polarization ray tracing matrices for the refraction at the entrance interface can be described by the following equations:

$$\mathbf{P_{in,A}} = \begin{pmatrix} t_{sA}\hat{\mathbf{E}}_\mathbf{A} & t_{pA}\hat{\mathbf{E}}_\mathbf{A} & \hat{\mathbf{S}}_\mathbf{A} \end{pmatrix} \cdot \begin{pmatrix} \hat{\mathbf{E}}_\mathbf{s} & \hat{\mathbf{E}}_\mathbf{p} & \hat{\mathbf{S}}_\mathbf{in} \end{pmatrix}^T. \tag{26}$$

$$\mathbf{P_{in,B}} = \begin{pmatrix} t_{sB}\hat{\mathbf{E}}_\mathbf{B} & t_{pB}\hat{\mathbf{E}}_\mathbf{B} & \hat{\mathbf{S}}_\mathbf{B} \end{pmatrix} \cdot \begin{pmatrix} \hat{\mathbf{E}}_\mathbf{s} & \hat{\mathbf{E}}_\mathbf{p} & \hat{\mathbf{S}}_\mathbf{in} \end{pmatrix}^T. \tag{27}$$

where $t_{ij}\,(i = s, p; j = A, B)$ is the amplitude transmission coefficient that the i polarization state of the incident ray in the isotropic medium refracts to the j polarization state of the refracted rays in the electro-optic crystal.

For the phase accumulation between the entrance interface and the exit interface, the optical path lengths of the two refracted rays should be incorporated into the polarization ray tracing matrices:

$$\mathbf{P_{OPL,A}} = \begin{pmatrix} e^{i\frac{2\pi}{\lambda} OPL_A}\hat{\mathbf{E}}_\mathbf{A} & \mathbf{0} & \hat{\mathbf{S}}_\mathbf{A} \end{pmatrix} \begin{pmatrix} \hat{\mathbf{E}}_\mathbf{A} & \hat{\mathbf{E}}_{\mathbf{A}\perp} & \hat{\mathbf{S}}_\mathbf{A} \end{pmatrix}^T, \tag{28}$$

$$\mathbf{P_{OPL,B}} = \begin{pmatrix} \mathbf{0} & e^{i\frac{2\pi}{\lambda}OPL_B}\hat{\mathbf{E}}_\mathbf{B} & \hat{\mathbf{S}}_\mathbf{B} \end{pmatrix} \begin{pmatrix} \hat{\mathbf{E}}_{\mathbf{B}\perp} & \hat{\mathbf{E}}_\mathbf{B} & \hat{\mathbf{S}}_\mathbf{B} \end{pmatrix}^T, \tag{29}$$

where $\mathbf{0}$ is a 3×1 zero vector; $\hat{\mathbf{E}}_{\mathbf{A}\perp}$ and $\hat{\mathbf{E}}_{\mathbf{B}\perp}$ are two pseudo polarization modes conveying no power and orthogonal to $\hat{\mathbf{E}}_\mathbf{A}$ and $\hat{\mathbf{E}}_\mathbf{B}$, respectively.

For the interaction between the ray and the exit interface, we also utilize two polarization ray tracing matrices to quantify the evolution of the polarization states at the exit interface:

$$\mathbf{P_{ex,A}} = \begin{pmatrix} t_{As}\hat{\mathbf{E}}_{\mathbf{As}} + t_{Ap}\hat{\mathbf{E}}_{\mathbf{Ap}} & \mathbf{0} & \hat{\mathbf{S}}_{\mathbf{ex,A}} \end{pmatrix} \cdot \begin{pmatrix} \hat{\mathbf{E}}_\mathbf{A} & \hat{\mathbf{E}}_{\mathbf{A}\perp} & \hat{\mathbf{S}}_\mathbf{A} \end{pmatrix}^T. \tag{30}$$

$$\mathbf{P_{ex,B}} = \begin{pmatrix} \mathbf{0} & t_{Bs}\hat{\mathbf{E}}_{\mathbf{Bs}} + t_{Bp}\hat{\mathbf{E}}_{\mathbf{Bp}} & \hat{\mathbf{S}}_{\mathbf{ex,B}} \end{pmatrix} \cdot \begin{pmatrix} \hat{\mathbf{E}}_{\mathbf{B}\perp} & \hat{\mathbf{E}}_\mathbf{B} & \hat{\mathbf{S}}_\mathbf{B} \end{pmatrix}^T. \tag{31}$$

Consequently, the total polarization ray tracing matrices to describe the evolution of the polarization states through the electro-optic crystal can be calculated by

$$\mathbf{P_{total,A}} = \mathbf{P_{ex,A}} \cdot \mathbf{P_{OPL,A}} \cdot \mathbf{P_{in,A}}. \tag{32}$$

$$\mathbf{P_{total,B}} = \mathbf{P_{ex,B}} \cdot \mathbf{P_{OPL,B}} \cdot \mathbf{P_{in,B}}. \tag{33}$$

Utilizing the orthogonal relations between the eigenmodes and substituting Eqs. (26)–(31) into Eq.(32) and Eq.(33), the total polarization ray tracing matrices can be expressed in (34) and (35), as shown at the bottom of the next page.

Up to now, we have obtained the total polarization ray tracing matrices for the ray A and the ray B through the electro-optic crystal. When these two rays exit the electro-optic modulator, we use 3×1 vectors $\mathbf{E_{total,A}}$ and $\mathbf{E_{total,B}}$ to characterize the exiting polarization vectors of the ray A and the ray B. These two vectors can be described by the following equations:

$$\mathbf{E_{total,A}} = \mathbf{P_N} \cdots \mathbf{P_{total,A}} \cdots \mathbf{P_1 E_0}, \tag{36}$$

$$\mathbf{E_{total,B}} = \mathbf{P_N} \cdots \mathbf{P_{total,B}} \cdots \mathbf{P_1 E_0}, \tag{37}$$

where the matrix $\mathbf{P_k}$ (k = 1, 2, . . . , N) is utilized to quantify the evolution of the polarization state through the polarizing optical element k.

Here, we assume that the amplitude distribution function of a light beam with arbitrary incident direction is $f(x, y)$. The exiting ray A and the exiting ray B are the rays at the center of the two exiting light beams whose amplitude distribution functions are $f_A(x, y)$ and $f_B(x, y)$, respectively. When the interference of the two exiting light beams is effectively total, the polarization vectors of the exiting light beams can be written as a sum:

$$\begin{aligned} \mathbf{E_{sum}} &= \mathbf{P_N} \cdots \left(\mathbf{P_{total,A}} + \mathbf{P_{total,B}}\right) \cdots \mathbf{P_1 E_0} \\ &= \mathbf{E_{total,A}} + \mathbf{E_{total,B}}. \end{aligned} \tag{38}$$

The intensity corresponding to the polarization vector $\mathbf{E_{sum}}$ can be expressed as

$$I_{sum} = (\mathbf{E_{sum}})^\dagger \mathbf{E_{sum}}. \tag{39}$$

where the † notation is used to represent the transpose of a matrix.

However, for a tilt incident light beam, these two exiting light beams are divergent and are partially interfered with each other. The combined polarization vector of the ray at the point (x, y) is:

$$\begin{aligned} &\mathbf{E}(x, y) \\ &= \mathbf{P_N} \cdots \left[f_A(x, y)\,\mathbf{P_{total,A}} + f_B(x, y)\,\mathbf{P_{total,B}}\right] \cdots \mathbf{P_1 E_0} \\ &= f_A(x, y)\,\mathbf{E_{total,A}} + f_B(x, y)\,\mathbf{E_{total,B}}. \end{aligned} \tag{40}$$

Then, the light intensity of the ray at the point (x, y) can be written as

$$\begin{aligned} I(x, y) = {} & f_A^2(x, y)\, I_{total,A} + f_B^2(x, y)\, I_{total,B} \\ & + f_A(x, y) f_B(x, y) \left(I_{sum} - I_{total,A} - I_{total,B}\right). \end{aligned} \tag{41}$$

where $I_{total,A}$ and $I_{total,B}$ are the intensity of the ray A and the ray B, which can be expressed as

$$I_{total,A} = \left(\mathbf{E_{total,A}}\right)^\dagger \mathbf{E_{total,A}}. \tag{42}$$

$$I_{total,B} = \left(\mathbf{E_{total,B}}\right)^\dagger \mathbf{E_{total,B}}. \tag{43}$$

Consequently, for a light beam incident with an arbitrary direction, the light flux Φ of the light beams exiting from the electro-optic modulator can be described by the following equation:

$$\begin{aligned} \Phi = {} & \left(I_{sum} - I_{total,A} - I_{total,B}\right) \int_{-\infty}^{+\infty} \int_{-\infty}^{+\infty} f_A(x, y) \\ & \times f_B(x, y)\, \mathrm{d}x\mathrm{d}y \\ & + I_{total,A} \int_{-\infty}^{+\infty} \int_{-\infty}^{+\infty} f_A^2(x, y)\, \mathrm{d}x\mathrm{d}y \\ & + I_{total,B} \int_{-\infty}^{+\infty} \int_{-\infty}^{+\infty} f_B^2(x, y)\, \mathrm{d}x\mathrm{d}y. \end{aligned} \tag{44}$$

III. RESULTS AND DISCUSSIONS

In section II, the theoretical model of the electro-optic modulator with three kinds of alignment errors has been established. As an application, we analyze the distribution characteristics of the exiting intensity of an electro-optic modulator under different alignment errors.

A z-cut lithium niobite (LN), a remarkable optical material, is chosen as the electro-optical crystal. The dimension of the LN crystal is 9 mm × 9 mm × 18.8 mm ($x \times y \times z$). A polarizer and an analyzer are placed on both sides of the lithium niobate crystal. The transmission axis of the polarizer is parallel to the X-axis of the global coordinate system, while the transmission axis of the analyzer is perpendicular to the X-axis. Besides, the α_G changes from 0 degree to 6 degree and ϕ_G changes from 0 degree to 360 degree. In order to facilitate the analysis, we consider that the exiting two light beams strike at the same pixel of a detector array due to the divergent distance is smaller than the pixel size of the detector array. As shown in FIGURE 3 and FIGURE 4, the theoretical results

of the exiting intensity are presented in a polar coordinate system.

Without the effect of the applied electric field, the LN crystal is uniaxial symmetry. FIGURE 3 (a) shows the distribution of the exiting intensity of the electro-optic modulator without alignment error and is a classic conoscopic interference pattern of the uniaxial crystals. The interference pattern consists of a set of concentric circles and a dark Maltese cross. The center of the concentric circles is the imaging point (the red dot) of the optical axis of the electro-optic modulator. The two centerlines of the dark Maltese cross are represented by the green straight lines in FIGURE 3 (a) and are oriented along the X-axis and the Y-axis, respectively. The intersection point of the two green straight lines represents the position of the LN crystal melatope. When the LN crystal is perfectly installed, the optical axis of the LN crystal coincides with the optical axis of the electro-optic modulator. Consequently, the position of the melatope coincides with the imaging point of the optical axis of the electro-optical modulator.

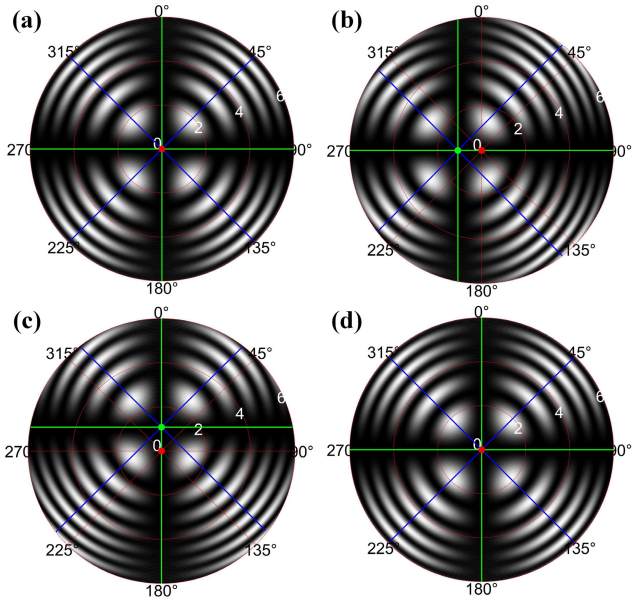

FIGURE 3. Distribution of the exiting intensity when the applied voltage is zero. (a) Without alignment error; (b) The horizontal error angle is 1 degree; (c) The vertical error angle is 1 degree; (d) The rotation error angle is 10 degree.

FIGURE 3 (b) and FIGURE 3 (c) describe the distributions of the exiting intensity of the field-free LN electro-optic modulator when the horizontal error angle is 1 degree and the vertical error angle is 1 degree, respectively. For these two alignment error conditions, the optical axis of the LN crystal does not coincide with the optical axis of the electro-optic modulator. The positions of the crystal melatope separate from the imaging point of the optical axis of the electro-optic modulator in the direction of the Y-axis and in the direction of the X-axis, respectively. FIGURE 3 (d) presents the distribution of the exiting intensity when the rotation error angle is 10 degree. Comparing FIGURE 3 (d) with FIGURE 3 (a), the distributions of the exiting intensity are the same for these two alignment conditions.

Furthermore, the centroids of each independent white area of a conoscopic interference pattern distribute on the two blue straight lines and the intersection point of the blue straight lines coincides with the intersection point of the green straight lines, as shown in FIGURE 3 (a)–(d). The angles between the X-axes and the blue straight lines are 45 degree and 135 degree, respectively. The directions of the green straight lines and the blue straight lines in FIGURE 3 (a)–(d) do not change with the alignment error angles, which means that the direction of the dark Maltese cross is determined by the transmission axes of the polarizer and analyzer when the applied voltage is 0V.

When the voltage applied on the LN crystal is the half-wave voltage, the LN crystal becomes biaxial symmetry and free principal dielectric axes of the crystals may rotate 45 degree around its optical axis to the field-induced principal dielectric axes. The distributions of the exiting intensity under different alignment errors are presented in FIGURE 4. Comparing FIGURE 4 (a) with FIGURE 3 (a), one can observe that the gray value of the center area of the conoscopic interference pattern changes from black to white and the concentric circles transform into ellipses when the half-wave voltage is applied on the LN crystal. However, the centroids of each independent white area distribute on the two blue straight lines shown in FIGURE 4 (a) and the intersection point of the two blue straight lines still coincides with the imaging point of the optical axis of the electro-optic modulator. The angles between these two blue straight lines and the X-axis are also 45 degree and 135 degree, respectively.

For the horizontal error and the vertical error, as shown in FIGURE 4 (b) and FIGURE 4 (c), the intersection points of the blue straight lines separate from the imaging point of the optical axis of the electro-optic modulator in the direction of the Y-axis and in the direction of the X-axis, respectively. FIGURE 4 (d) describes the distribution of the exiting intensity of the electro-optic modulator when the rotation error angle is 10 degree. Unlike the distribution characteristics of the exiting intensity of the field-free electro-optic modulator shown in FIGURE 3 (d), the exiting intensity is seriously affected by the rotation error angle when the voltage applied on the LN crystal is the half-wave voltage. Besides,

$$\mathbf{P}_{\mathbf{total,A}} = \left[t_{sA} e^{i\frac{2\pi}{\lambda} OPL_A} \left(t_{As}\hat{\mathbf{E}}_{\mathbf{As}} + t_{Ap}\hat{\mathbf{E}}_{\mathbf{Ap}} \right) \quad t_{pA} e^{i\frac{2\pi}{\lambda} OPL_A} \left(t_{As}\hat{\mathbf{E}}_{\mathbf{As}} + t_{Ap}\hat{\mathbf{E}}_{\mathbf{Ap}} \right) \quad \hat{\mathbf{S}}_{\mathbf{ex,A}} \right] \left(\hat{\mathbf{E}}_{\mathbf{s}} \quad \hat{\mathbf{E}}_{\mathbf{p}} \quad \hat{\mathbf{S}}_{\mathbf{in}} \right)^T. \tag{34}$$

$$\mathbf{P}_{\mathbf{total,B}} = \left[t_{sB} e^{i\frac{2\pi}{\lambda} OPL_B} \left(t_{Bs}\hat{\mathbf{E}}_{\mathbf{Bs}} + t_{Bp}\hat{\mathbf{E}}_{\mathbf{Bp}} \right) \quad t_{pB} e^{i\frac{2\pi}{\lambda} OPL_B} \left(t_{Bs}\hat{\mathbf{E}}_{\mathbf{Bs}} + t_{Bp}\hat{\mathbf{E}}_{\mathbf{Bp}} \right) \quad \hat{\mathbf{S}}_{\mathbf{ex,B}} \right] \left(\hat{\mathbf{E}}_{\mathbf{s}} \quad \hat{\mathbf{E}}_{\mathbf{p}} \quad \hat{\mathbf{S}}_{\mathbf{in}} \right)^T. \tag{35}$$

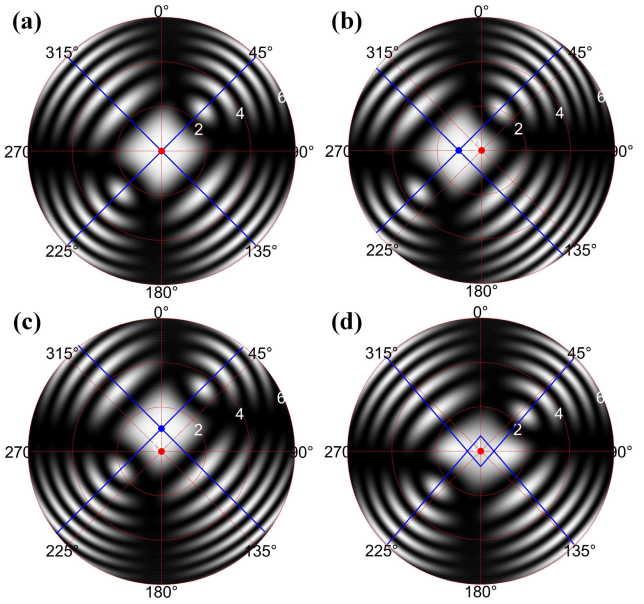

FIGURE 4. Distribution of the exiting intensity when the applied voltage is the half-wave voltage. (a) Without alignment error; (b) The horizontal error angle is 1 degree; (c) The vertical error angle is 1 degree; (d) The rotation error angle is 10 degree.

the centroids of each independent white area distribute on four blue straight lines shown in FIGURE 4 (d). These four intersection points of the blue straight lines are symmetric distribution around the imaging point of the optical axis of the electro-optic modulator.

The distribution characteristics of the exiting intensity shown in FIGURE 3 and FIGURE 4 are useful to achieve high precision alignment of the electro-optic modulators in practical applications. The schematic diagram of the experimental setup designed for recording the exiting intensity of the electro-optic modulator based on the LN crystal is presented in FIGURE 5. A collimated laser beam is produced by a 660-nm-wavelength diode laser and corresponding collimator. Two linear polarizers with high extinction ratio and high laser damage threshold are chosen as the polarizer and analyzer. The extinction ratios are larger than 10000:1 and the laser damage thresholds is up to 25W/cm^2. The polarizer is used to transform the polarization state of the collimated laser beam to polarize along the X-axis and the radius of the laser beam is controlled by the stop. The laser beam is then focused onto the entrance interface of the LN crystal by lens 1 which is confocal with lens 2. The laser beam exiting from the LN crystal is collimated by lens 2 and then propagates through the analyzer. The exiting laser beam is received by the camera.

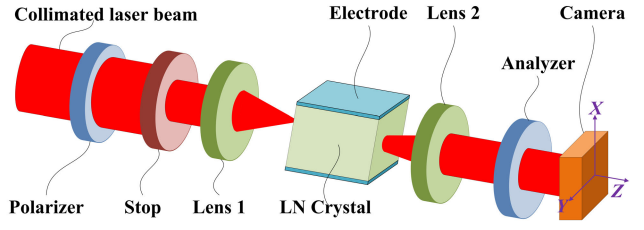

FIGURE 5. Schematic diagram of the experimental setup.

As described in FIGURE 3, when the applied voltage is zero, the directions of the blue straight lines that consist of the centroids of each independent white area do not affected by the alignment errors. Before the electric field is applied on the LN crystal, we rotate the polarizer and the analyzer around the optical axis of the electro-optic modulator to make sure the angles between the X-axis and the straight lines that consist of the centroids are 45 degree and 135 degree. Consequently, the transmission axes of the polarizer and the analyzer are aligned with the X-axis and the Y-axis, respectively. Then the half-wave voltage is applied on the LN crystal and the crystal is rotated around the optical axis of the electro-optic modulator to make sure the centroids distribute on two straight lines.

The method to determine the directions of the straight lines consist of the centroids is presented in FIGURE 6. First, the gray image produced by the camera is processed by the binarization algorithm, open-operation algorithm, close-operation algorithm, and median filtering algorithms. Then, the centroids are extracted from each independent white area and are marked with the blue dots. Finally, the centroids are fitted with the blue straight lines. The angles between the X-axis and the blue straight lines in FIGURE 6 (a) are 45.0062 degree and 135.0051 degree, respectively. The angles between the X-axis and the blue straight lines in FIGURE 6 (b) are 45.0078 degree and 135.0042 degree, respectively. As far as we know, the azimuth measurement accuracy of the commercial off-the shelf polarimeters are generally less than 0.25°. Consequently, the theoretical alignment precision of this method is much higher than that of the commercial off-the-shelf polarimeters.

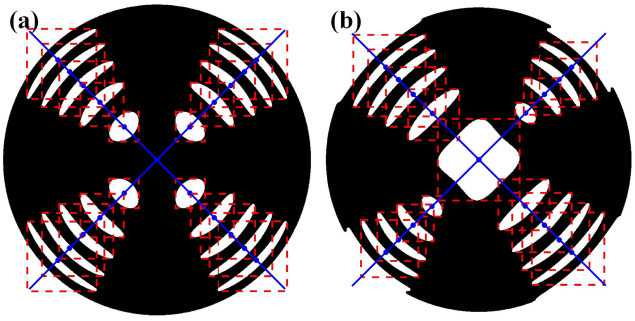

FIGURE 6. Determination of the directions of the straight lines that consist of the centroids of each independent white area: (a) The applied voltage is zero; (b) The applied voltage is the half-wave voltage.

In order to align the transmission axes of the polarizer and the analyzer with the X-axis and the Y-axis, we first place the analyzer before the stop and utilize a power meter to measure the light beams exiting from the analyzer. Then, we rotate the analyzer around the Z-axis until the output result of the power meter is the smallest to make sure the orthogonal relationship between the transmission axis of the polarizer and the transmission axis of the analyzer. Afterwards, we use the camera to record the exiting intensity and utilize the method described in Figure 6 (a) to extract the angles between X-axis and the two straight lines. Finally, repeat the procedures to make

sure the angles between X-axis and the two straight lines are gradually close to 45 degree and 135 degree. In order to make sure the centroids distribute on two straight lines, when the half-wave voltage is applied, we utilize the method described in Figure 6 (b) to extract the angle between the X-axis and the straight lines. Then, we rotate the lithium niobate crystal until the angle between the X-axis and the straight lines are gradually close to 45 degree and 135 degree.

It is worth noting that the measurement uncertainty of the power meter may affect the adjustment of the orthogonal relationship between the transmission axis of the polarizer and the transmission axis of the analyzer. Moreover, the polarizer and the analyzer are mounted in two continuous rotation mounts which offer 2° graduation marks. It is difficult to rotate the polarizer or the analyzer at a very small angle. In the experiments, when the applied voltage is 0 Vπ, the angles between the X-axis and the two straight lines are gradually close to 44.89 degree and 134.97 degree. When the half-wave voltage is applied, the angles between the X-axis and the two straight lines are gradually close to 45.15 degree and 134.83 degree. If the polarizer and the analyzer are mounted on high precision rotation mounts, higher alignment precision can be achieved in the experiments. The experimental exiting intensity results of the electro-optic modulator are presented in FIGURE 7. Comparing FIGURE 7 with FIGURE 3(a) and FIGURE 4 (a), the experimental intensity results strongly agree with the theoretical intensity results, which indicates the validity of the theoretical model for the electro-optic modulator.

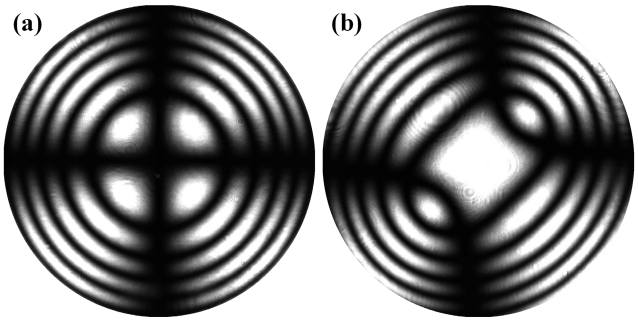

FIGURE 7. The experimental exiting intensity results of the high precision aligned electro-optic modulator. (a) The applied voltage is zero; (b) The applied voltage is the half-wave voltage.

IV. CONCLUSION

Electro-optic modulators are an integral part of a wide range of modern optical systems. In order to provide theoretical guidance in aligning the modulators, a model for the electro-optic modulator with three kinds of alignment errors is established in this paper. Utilizing the model, the distribution characteristics of the exiting intensity of an electro-optic modulator based on lithium niobite crystal are discussed. Regardless of whether or not a voltage is applied on the modulator, the horizontal error angle and the vertical error angle will induce a horizontal offset and vertical offset of the conoscopic interference patterns. When the applied voltage is zero, the rotation error angle does not influence the distribution of the exiting intensity. However, the exiting intensity is seriously affected by the rotation error angle when the voltage applied on the LN crystal is the half-wave voltage. Based on the distribution characteristics of the exiting intensity, the LN electro-optic modulator is accurately aligned and the experimental results agree very well with the corresponding theoretical results.

REFERENCES

[1] M. Li and H. X. Tang, "Strong Pockels materials," *Nature Mater.*, vol. 18, no. 1, pp. 9–11, Jan. 2019.
[2] A. Rueda, "Efficient microwave to optical photon conversion: An electro-optical realization," *Optica*, vol. 3, no. 6, pp. 597–604, Jun. 2016.
[3] A. J. Bowman, B. B. Klopfer, T. Juffmann, and M. A. Kasevich, "Electro-optic imaging enables efficient wide-field fluorescence lifetime microscopy," *Nature Commun.*, vol. 10, no. 1, p. 4561, Oct. 2019.
[4] B. Han, W. Zhao, X. Xie, Y. Su, W. Wang, and H. Hu, "Influence of laser linewidth and polarization modulator length on polarization shift keying for free space optical communication," *Opt. Express*, vol. 23, no. 7, pp. 8639–8649, Apr. 2015.
[5] P. Zhang, X. Du, J. Zhao, Y. Song, and H. Chen, "High resolution flash three-dimensional LIDAR systems based on polarization modulation," *Appl. Opt.*, vol. 56, no. 13, pp. 3889–3894, May 2017.
[6] S. Jo, H. J. Kong, H. Bang, J.-W. Kim, J. Kim, and S. Choi, "High resolution three-dimensional flash LIDAR system using a polarization modulating Pockels cell and a micro-polarizer CCD camera," *Opt. Express*, vol. 24, no. 26, pp. A1580–A1585, Dec. 2016.
[7] P. F. McManamon, P. S. Banks, J. D. Beck, D. G. Fried, A. S. Huntington, and E. A. Watson, "Comparison of flash lidar detector options," *Opt. Eng.*, vol. 56, no. 3, Mar. 2017, Art. no. 031223.
[8] H. Song, X. Qi, W. Zou, Z. Zhong, and S. A. Burns, "Dual electro-optical modulator polarimeter based on adaptive optics scanning laser ophthalmoscope," *Opt. Express*, vol. 18, no. 21, pp. 21892–21904, Oct. 2010.
[9] Y. Song, K. Zhang, Q. Hao, and J. P. Rolland, "Modeling and characterization of the electrostatic coupling intra-body communication based on Mach-Zehnder electro-optical modulation," *Opt. Express*, vol. 20, no. 12, pp. 13488–13500, Jun. 2012.
[10] M. Izdebski, W. Kucharczyk, and R. E. Raab, "Application of the Jones calculus for a modulated double-refracted light beam propagating in a homogeneous and nondepolarizing electro-optic uniaxial crystal," *J. Opt. Soc. Amer. A, Opt. Image Sci.*, vol. 21, no. 1, pp. 132–139, Jan. 2004.
[11] J. R. Mackey, K. K. Das, S. L. Anna, and G. H. McKinley, "A compact dual-crystal modulated birefringence-measurement system for microgravity applications," *Meas. Sci. Technol.*, vol. 10, no. 10, pp. 946–955, 1999.
[12] L. J. Cervantes, D. I. Serrano-Garcia, Y. Otani, and B. Cense, "Mueller-matrix modeling and characterization of a dual-crystal electro-optic modulator," *Opt Express*, vol. 24, no. 21, pp. 24213–24224, Oct. 2016.
[13] P. Zhang, X. Du, Y. Song, J. Wu, and J. Sun, "Phase shift formulas in electro-optical crystals with an arbitrary incident direction," *J. Phys. D, Appl. Phys.*, vol. 53, no. 9, Dec. 2019, Art. no. 095306, doi: 10.1088/1361-6463/ab56c4.
[14] R. A. Chipman, "Mechanics of polarization ray tracing," *Opt. Eng.*, vol. 34, no. 6, pp. 1636–1645, Jun. 1995.
[15] G. Yun, K. Crabtree, and R. A. Chipman, "Three-dimensional polarization ray-tracing calculus I: Definition and diattenuation," *Appl. Opt.*, vol. 50, no. 18, pp. 2855–2865, Jun. 2011.
[16] W. S. T. Lam, "Anisotropic ray trace," Ph.D. dissertation, College Opt. Sci., Univ. Arizona, Tucson, AZ, USA, 2015.

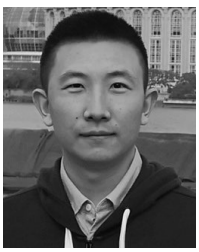

PENG ZHANG was born in Hubei, China, in 1990. He received the M.S. degree from AUAF, China, in 2015. He is currently pursuing the Ph.D. degree with Space Engineering University, Beijing, China. His research interests include ray tracing in electro-optic crystals and high resolution flash.

XIAOPING DU was born in Hebei, China, in 1966. She received the Ph.D. degree from the Beijing Institute of Technology, China, in 2004. She has been a Professor with Space Engineering University, Beijing, China. Her current research interests include space mission analysis, high-resolution flash lidar, ray tracing in electro-optic crystals, and machine learning.

YISHUO SONG was born in Beijing, China, in 1985. He received the Ph.D. degree from Space Engineering University, Beijing, China, in 2014. He has been a Lecturer with Space Engineering University. His current research interests include high resolution flash lidar, ray tracing in electro-optic crystals, and electro-optic devices.